A Comparison of BRDF Models for the Normalization of Satellite Optical Data to a Standard Sun-Target-Sensor Geometry

Rasim Latifovic, Josef Cihlar, and Jing Chen, *Member, IEEE*

***Abstract*—Climate change studies require consistent, long time series, surface reflectance data. The characterization of the bidirectional reflectance distribution function (BRDF) is important for normalizing the solar radiation reflected from the earth's surface. We evaluated four BRDF models to identify the preferred approach to the normalization of multiyear National Oceanic and Atmospheric Administration Advanced Very High Resolution Radiometer (AVHRR) and SPOT4-VEGETATION (VGT) composite images to a common illumination and viewing geometry. Four models by the following authors were included: Walthall, Roujean, Ross–Li, and a new nonlinear temporal angular model (NTAM). NTAM accounts for hotspot effects and also responds to seasonal changes in land cover properties (using vegetation indexes as surrogate temporal measures). We compared the performance of the models under different scenarios of coefficient derivation and model application including model ability to reproduce theoretical BRDF curves, model consistency in single, multiyear, and incomplete sampling schemes, and comparison of AVHRR and LANDSAT Thematic Mapper surface reflectance prior and after BRDF normalization. We found that in all the tests, NTAM yielded the best fits between the observed and estimated values. NTAM requires eight coefficients and a lengthier iterative procedure to derive the coefficients, but the resulting coefficients are applied to the entire growing season rather than one temporal window. NTAM also performed well for different sensors (AVHRR, VGT) and geographic areas (Canada, east Asia, southern United States). Our results contradict the often-encountered perception that semiempirical BRDF models for angular normalization are all similarly effective, and the research on this topic is mature. We also describe a procedure for routine normalization of satellite optical data. For northern ecosystems, the NTAM coefficients derived from AVHRR and VGT data for Canada are available via *ftp://ccrs.nrcan.gc.ca*.**

***Index Terms*—BRDF normalization, image processing, remote sensing.**

I. Introduction and Objectives

THE SUN-TARGET-sensor geometry effects inherent in optical satellite measurements are a potential source of biophysical information about terrestrial ecosystems [18]. To realize this potential, it is necessary to obtain a sufficient number of satellite measurements with a range of sun-target-sensor geometries while the target remains unchanged. Although this is a desirable objective, and new programs are oriented in this direction (e.g., the Polarization and Directionality of the Earth's Reflectances instrument, the Moderate Resolution Imaging Spectroradiometer (MODIS)/Multi-angle Imaging SpectroRadiometer combination on Terra, the proposed European Space Agency Panchromatic Remote Sensing Instrument for Stereo Mapping mission), it is not always achievable. In particular, sampling provided by previous and existing satellite systems has been only marginally sufficient for this purpose. Our experience with Advanced Very High Resolution Radiometer (AVHRR) data from northern latitudes also indicates that, even with multiple sensors and an enlarged temporal window, routine acquisition of a sufficient number of clear-sky observations remains a major challenge.

When the objective of a study is not retrieval of biophysical parameters from bidirectional reflectance distribution function (BRDF) characteristics but a comparative quantitative analysis, the potential fluctuations due to BRDF limit the ability to monitor ecosystems and track vegetation dynamics. An alternative, although perhaps suboptimal, use of bidirectional information is to employ multiple measurements of the same pixel at different angles and times to remove bidirectional effects from the data [20]. This approach does not directly generate new information about the target, but it does provide at least one good measurement for the time interval of interest that is free from directional effects. It is achieved by characterizing the anisotropy of the target, described by the BRDF. Various investigators have employed this approach in the past [5], [9], [12]–[14], [16], [28]. Because detailed multiangle measurements at desired spatial and temporal resolutions are often not available, this approach is useful for normalizing temporal series to a common viewing geometry from archived data sources as well as for new data acquired by coarse resolution sensors as SPOT/VEGETATION (VGT) and MODIS.

To normalize remote sensing data to a standard geometry, a sound model of the bidirectional reflectance behavior of various surfaces is required. This is an area of very active research (see [18] for review). The primary objectives of this study were: 1) to identify a suitable BRDF model for northern ecosystems applicable to AVHRR and similar data and 2) to define a procedure for deriving the model parameters for an area to accurately correct multiyear series of composite images. The desired model should be applicable to the entire growing season, should be robust in terms of wide range of sun and viewing angles as well as phenological changes, and should reproduce actual satellite observations as closely as possible. In addition, the model should be temporally consistent, i.e., model parameters derived from

Manuscript received April 5, 2001; revised January 7, 2003.

R. Latifovic and J. Cihlar are with the Natural Resource Canada CCRS, Ottawa, ON K1A 0Y7, Canada (e-mail: Rasim.Latifovic@ccrs.nrcan.gc.ca; Josef.Cihlar@ccrs.nrcan.gc.ca).

J. Chen is with the Department of Geography and Program and Planning, University of Toronto, Toronto, ON M5S 3G3, Canada (e-mail: chenj@geog.utoronto.ca).

Digital Object Identifier 10.1109/TGRS.2003.811557

previous growing seasons should be extendable to the subsequent seasons so the normalization may be performed in near real time. It should also be relatively simple so that model parameters may be easily updated. The model needs to be robust in terms of the variable spatial footprint, e.g., as insensitive as possible to the mixed land cover nature of satellite pixels. The model should perform well in operational processing of large data volumes representing a variety of conditions (e.g., significant data noise or other limitations, strong hotspot effects, or heterogeneous and temporally variable surfaces).

Ideal BRDF model characteristics are difficult to derive with physically based models. Physical BRDF models are complex, and inversion procedures must be used to estimate values of their parameters. They are also computationally demanding and are impractical for frequent processing of large images. A significant number of parameters are required for physical models, which assumes *a priori* information about the scene. It is, therefore, desirable to derive parameters required in simple models from the data itself.

In an attempt to provide accurate corrections for multiyear series of AVHRR composite data for northern ecosystems, the Canada Centre for Remote Sensing conducted several studies aimed at characterizing the BRDF behavior of boreal landscapes [2], [3], [16], [28]. This research generally followed the modeling approach of the semiempirical kernel driven BRDF model originated by Roujean *et al.* [24] in which the reflectance is assumed to consist of three additive kernels describing isotropic scattering, geometric shadowing, and volume scattering, respectively. The kernels were derived from approximations to the principles of geometrical optics and from simplifications of radiative transfer theory, defining the BRDF shape in terms of solar illumination and sensor viewing angles. Kernel-based approaches have also been employed by various other investigators [1], [17], [21], [22], [26], and they have become the main strategy employed for Earth Observing System Terra products through inversion of multiple measurements [1], [30]. In addition to testing several well-known models, we have also developed a new model by combining aspects of existing models and found a way to account for seasonal variability in BRDF.

II. Methodology

The overall methodology consisted of selection of several candidate models, preparation of the AVHRR and VGT datasets, derivation of model coefficients and statistics for each model, and comparison of the measured and predicted AVHRR and VGT values.

A. Models

We have selected three kernel-based models that represent the range of currently used approaches to BRDF modeling, and added a model called the nonlinear temporal angular model (NTAM). Models selected for the comparison are 1) modified Walthall model (MWM) [27] (an empirical BRDF kernel-driven model with basic trigonometric expressions as kernels), 2) semiempirical Roujean model (RM) [24] with two kernels, and 3) Ross–Li Model (RLM) [20], [25] based on randomly placed spheroids. Each model has been designed to address some specific BRDF characteristics. For example, the MWM is a statistically based model, which, while it can be optimally adjusted to match a sample dataset, does not have a strong physical basis for its assumptions, and thus makes it more difficult to extrapolate beyond the sample space. The Ross–Li and Roujean models are semiphysical models but do not account for seasonality or hot spots. The basic equations for the models are provided below.

RM:

$$\rho(\theta_s,\theta_v,\phi) = a_0 + a_1 f_1(\theta_s,\theta_v,\phi) + a_2 f_2(\theta_s,\theta_v,\phi). \quad (1)$$

MWM:

$$\rho\left(\theta_s,\theta_v,\phi\right) = a_0\left(\theta_v^2+\theta_s^2\right) + a_1\theta_v^2\theta_s^2 + a_2\cos\left(\phi\right) + a_4. \quad (2)$$

RLM:

$$\rho(\theta_s,\theta_v,\phi) = a_0 + a_1 K_{\mathrm{vol}}(\theta_s,\theta_v,\phi) + a_2 K_{\mathrm{geo}}(\theta_s,\theta_v,\phi). \quad (3)$$

NTAM:

$$\rho_i(\theta_s,\theta_v,\phi,\Delta_i) = \begin{bmatrix} 1+\left(a_1+a_2(1-\Delta_i)+a_3(1-\Delta_i)^2\right) \\ *f_1\left(\theta_s,\theta_v,\phi\right)+\left(a_4+a_5\Delta_i+a_6\Delta_i^2\right) \\ *f_2(\theta_s,\theta_v,\phi) \end{bmatrix} *(1+a_7 e^{-\xi/\pi a_8}) \quad (4)$$

where

$$\cos\xi = \cos\theta_s\cos\theta_v + \sin\theta_s\sin\theta_v\cos\phi$$

$$f_1(\theta_s,\theta_v,\phi) = \frac{1}{2\pi}\left[(\pi-\phi)\cos\phi+\sin\phi\right]\tan\theta_s\tan\theta_v - \frac{1}{\pi}\left(\tan\theta_s+\tan\theta_v + \sqrt{\tan^2\theta_s+\tan^2\theta_v-2\tan\theta_s\tan\theta_v\cos\phi}\right)$$

$$f_2\left(\theta_s,\theta_v,\phi\right) = 4/3\pi * 1/\cos\theta_s + \cos\theta_v\left[(\pi/2-\xi)\cos\xi+\sin\xi\right] - 1/3$$

and

$$\begin{aligned} \Delta_1 &= \rho_2-\rho_1/\rho_1+\rho_2 \quad \text{(for the visible band)} \\ \Delta_2 &= \rho_2-\rho_1 \quad \text{(for the near-infrared band)} \\ K_{\mathrm{vol}} &= f_1 \\ K_{\mathrm{geo}} &= O\left(\theta_s,\theta_v,\phi\right) - \sec\theta_s' - \sec\theta_v' + \frac{1}{2}\left(1+\cos\xi'\right)\sec\theta_s'\sec\theta_v' \\ O &= \frac{1}{\pi}\left(t-\sin t\cos t\right)\left(\sec\theta_s'+\sec\theta_v'\right) \\ \cos t &= \frac{h}{b}\frac{\sqrt{D^2+\left(\tan\theta_s'\tan\theta_v'\right)^2}}{\sec\theta_s'+\sec\theta_v'} \\ D &= \sqrt{\tan^2\theta_s'+\tan^2\theta_v'-2\tan\theta_s'\tan\theta_v'\cos\phi} \\ \theta_s' &= \tan^{-1}\left(\frac{b}{r}\tan\theta_2\right) \\ \theta_v' &= \tan^{-1}\left(\frac{b}{r}\tan\theta_v\right) \\ \cos\xi' &= \cos\theta_s'+\sin\theta_s'+\sin\theta_v'\cdot\cos\phi \end{aligned}$$

where

- θ_s, θ_v, ϕ solar zenith angle, view zenith angle, and the difference in azimuth angles between the sun and the sensor;
- f_1 volume scattering component, which describes the "shape" of the BRDF due to the scattering of radiation within the "volume" of the surface material and a weighting factor for this kernel that is expressed in terms of $(1 - \Delta_i)$ and is related to biophysical parameters;
- f_2 surface scattering component, which accounts for the shadowing and occlusion effects based on geometric optics; a weighting factor for this kernel is expressed in terms of Δ_i, which is in turn related to biophysical parameters. The introduction of Δ_i to the model makes it possible to track seasonal variations of BRDF shapes with a set of time-invariant coefficients a_i;
- K_{geo} Li sparse kernel with an assumption of a sparse ensemble of surface objects casting shadows on the background; the kernel is derived from the geometric-optical mutual shadowing BRDF model [17];
- O overlap between the view and solar shadows;
- h, b, r crown height and shape parameters.

NTAM is designed specifically to facilitate normalization of optical satellite measurements to a standard geometry. For this purpose, it is desirable that the same model handles different land cover types and different time periods equally effectively, and that its coefficients be easily obtained for a given dataset. NTAM geometric and volume scattering components are modeled using the kernel approach of Roujean *et al.* [24], the hot spot expression proposed by Chen and Cihlar [2], and a replacement for the α parameter of Roujean *et al.* [24], which quantifies the relative importance of geometric and volume scattering. The temporal dimension is approximated by polynomials, which account for 1) the varying amount of green leaf area in the course of the growing season and 2) the temporal patterns of geometric and volume scattering as influenced by land cover characteristics. The spatial pattern of BRDF retrievals shows that open land cover types (urban, suburban, and interurban regions) exhibit directional scattering that is well modeled by geometric optics of shadow casting. The directional reflectance of continuous forest areas is dominated by volume scattering [10]. Therefore, the temporally variable proportions of geometric and volume scattering are directly related to the amount of vegetation described by a polynomial function of a vegetation index (VI). We used the normalized difference vegetation index (NDVI) for the visible bands, and the difference between near-infrared (NIR) and red reflectances for NIR band. These two indexes yielded the highest coefficients of determination (r^2) between model estimated and observed AVHRR data.

A preliminary evaluation of NTAM's potential to reproduce theoretical BRDF functions in comparison to other models was performed on simulated data obtained with the 4-Scale geometric-optical canopy radiative transfer model [2]. The 4-Scale model has been shown to closely reproduce measured BRDF behavior of forest canopies [15]. The curve in Fig. 1 shows BRDF values for high-density coniferous forest simulated with 4-Scale. The coefficients were derived for each of the four models after sampling the 4-Scale curve (sampling 80 points); each model and its coefficients were then used to reproduce the original curves. The results confirm the well-known inability of linear models to describe the hotspot near the solar illumination direction. This has been achieved in NTAM with the relatively simple formulation of the hotspot effect at the cost of a larger number of model coefficients and model nonlinearity.

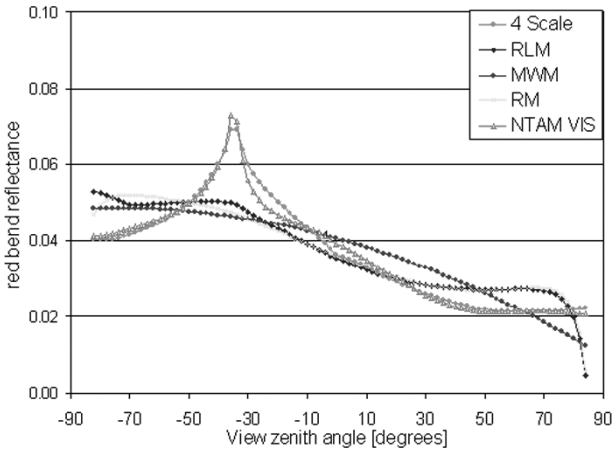

Fig. 1. Comparison of BRDF models' capability to match a "theoretical" BRDF shape, derived with 4-Scale, a detailed canopy BRDF model.

A further evaluation of NTAM was carried out by comparing uncorrected and corrected reflectance values of AVHRR composite data from 1998 with eight spatially and temporally coincident LANDSAT Thematic Mapper (TM) scenes. Fig. 2 compares an AVHRR ten-day composite image (channel 1, 1998/08/01–10) and LANDSAT TM (NIR band, path 15/row 29, 1998/08/02) before and after normalization. The TM data were atmospherically corrected [4] and resampled to equivalent 1-km^2 pixels by applying an approximate modulation transfer function (MTF) for AVHRR sensor but without considering sensor spectral response differences. The NIR AVHRR measurements prior to BRDF normalization (x axis), when plotted against the corresponding LANDSAT TM values [Fig. 2(a)], show two distinct distributions. As evidenced by Fig. 2(b), these distributions reflect the origin of the AVHRR pixels from two orbits with different view zenith angles. After normalizing BRDF to a common viewing geometry ($\theta_s = 45^\circ$, $\theta_v = 0^\circ$, $\Delta\phi = 0^\circ$), the differences disappeared, and the estimated AVHRR reflectance values correspond more closely to the simulated ones with TM data [Fig. 2(c)].

The following (Sections II-B and C) describes the components needed in using a BRDF model to normalize multiangle seasonal measurements to a standard geometry. First, the coefficients are obtained for individual land cover categories. We have used a land cover map for this purpose, but this is not a strict requirement as will be discussed later. Subsequently, normalization to a standard geometry is performed for any image composite of the area using land cover information, a lookup table (LUT) containing model coefficients for each cover type, and the pixel imaging geometry.

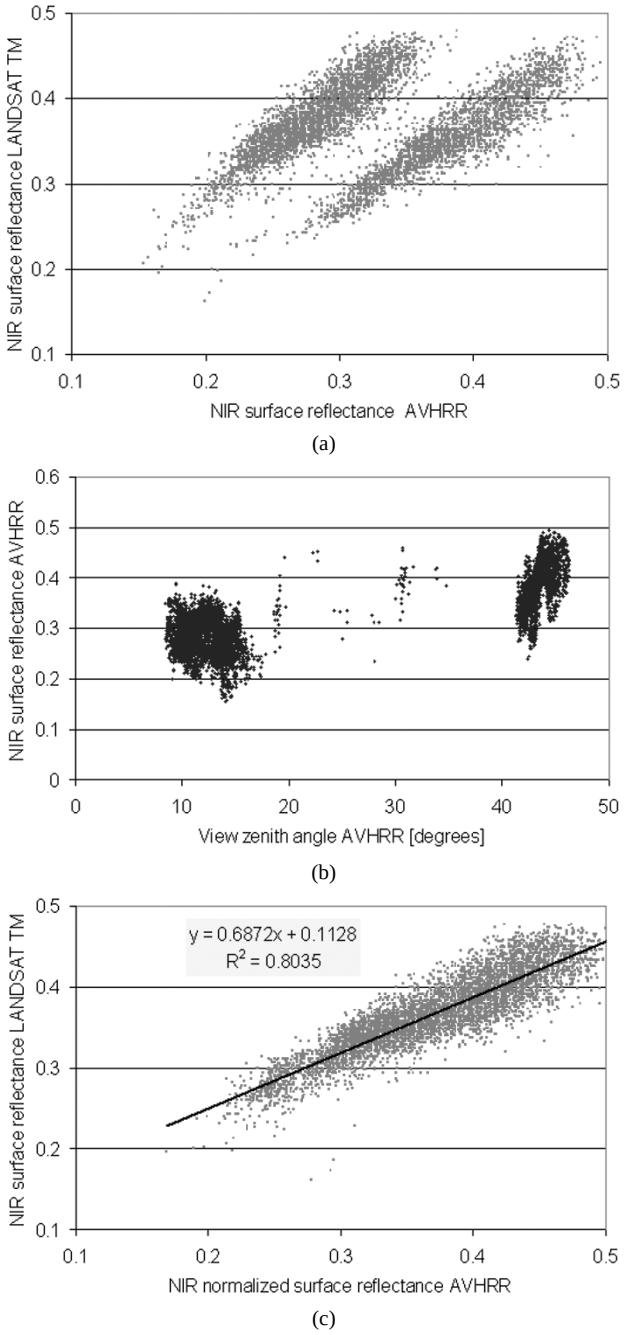

Fig. 2. Performance evaluation for the nonlinear model (NTAM). (a) Scatter plot of AVHRR NIR reflectance (1998/08/01–10) against TM NIR reflectance (scene path 19, row 29, 1998/08/02) prior to BRDF normalization. (b) Scatter plot of AVHRR NIR reflectance against satellite zenith angle in the AVHRR composite. (c) Scatter plot of AVHRR NIR reflectance composite against TM NIR reflectance after BRDF normalization.

B. Data Description

To derive coefficients and compare BRDF models, we employed Canada-wide National Oceanic and Atmospheric Administration (NOAA) AVHRR composite images. The initial dataset consisted of 20 ten-day image composites, between April 11 and October 31, including growing seasons from 1993 to 1999. The composite data were produced by the Geocoding and Compositing (GeoComp) system [32]. GeoComp performs calibration for the five AVHRR bands using time-dependent gain and offset coefficients [31] for channels 1 and 2 and onboard calibration data for channels 3 to 5. Satellite data are registered to ground control points using high-resolution image chips and resampled by a modified Kaiser 16-point kernel. The registered images are further used in a compositing procedure based on the maximum NDVI criterion. For each ten-day composite, GeoComp generates ten channels of data in Lambert conformal conic projection (LCC) (49° N and 77° N as the standard parallels, 95° W as the reference meridian). For the selected pixels, composite channels include five AVHRR radiance bands, NDVI, view zenith angle, solar zenith angle, relative azimuth angle between the sun and the satellite, and the satellite acquisition date.

The initial composite datasets were further processed using a postseasonal processing chain based on ABC3v2 methodology [6]–[8], which performs the following:

1) generation of a quality mask with missing pixels, view zenith, and sun zenith angle restrictions;
2) data recalibration using the latest AVHRR calibration coefficients (*http://www.ccrs.nrcan.gc.ca*);
3) computation of the top-of-the-atmosphere (TOA) reflectance;
4) atmospheric correction of AVHRR channels 1 and 2 using SMAC algorithm [23];
5) identification of cloudy, partly cloudy and snow covered pixels.

The simplified method for atmospheric corrections (SMAC) [23] was employed for atmospheric correction of the satellite measurements. SMAC accounts for gaseous transmission as well as for absorption, aerosol, and Rayleigh scattering. The method requires vertically integrated amounts of different gaseous components, sun zenith angle θ_s, view zenith angle θ_v, relative azimuth angle $\Delta\phi$, and the value of aerosol optical depth at 550 nm for each pixel. For atmospheric parameters, we used daily (total column) ozone data obtained by the Total Ozone Mapping Spectrometer on Meteor 3 [35] for atmospheric pressure, and integrated column water data from the National Center for Atmospheric Research reanalysis [36] estimates for 6-h periods on a 2.5° by 2.5° grid. A constant value was used for aerosol optical depth. This was necessitated by the lack of better data and was justified by sunphotometer measurements acquired at several sites across Canada over several years by the AEROCAN aerosol network. The value of 0.06 at 550 nm gives a good single-value representation of the aerosol optical depth [11].

In addition to the AVHRR data, we also evaluated models using VGT composite images over Canada. The ten-day synthesis data (S10 product) were provided by the VITO Centre (*http://www.vgt.vito.be*). As provided, each ten-day VGT composite contains apparent surface reflectance in four spectral bands. The S10 product also includes NDVI, sun-target-sensor geometry, reference date and time of the selected pixel, and quality information on the composite status map. For this study, the images were reprojected from the original Plate Carree projection into LCC. The initial composite datasets were further processed using the correction procedure designed for VGT composite data. The following preprocessing steps were carried out:

TABLE I
LAND COVER TYPES USED IN THE BRDF MODELING

Label	Index	Land cover type
CSFHD	1	Coniferous southern forest high to medium density
CNFMD	2	Coniferous northern forest medium density
CSFLD	3	Coniferous southern forest low density
CNFLD	4	Coniferous northern forest low density
BF	5	Broadleaf forest
MCF	6	Mixed coniferous forest
MIF	7	Mixed intermediate forest
B	8	Burns
OL	9	Open land
G	10	Grassland
CL	11	Crop Land
ML	12	Mosaic Land
UB	13	Urban and Built-up
S	14	Snow

1) identification of cloudy, partly cloudy and snow-covered pixels to produce a pixel contamination mask;
2) BRDF model coefficients derivation;
3) normalization to common sun-target-sensor geometry;
4) replacement of contaminated pixels through temporal interpolation.

C. Computation of BRDF Model Coefficients

The analysis was conducted on the AVHRR image composites for the Canadian landmass and the growing seasons of 1993 to 1994 (acquired by NOAA 11) and 1995 to 1999 (acquired by NOAA 14). As a second sensor, VGT S10 products from 1998 and 1999 were used. The BRDF model coefficients were computed for each year combination separately, using a sample of surface reflectance observations. The sampling procedure was implemented to ensure that all the datasets used in the calculation have a representative range of sun and view zenith angles, a similar number of pixels for each land cover type, and an even spatial and temporal distribution. The sampling procedure used the land cover map of Canada [33] and quality masks to extract clear-sky pixel surface reflectance in each spectral band, and the corresponding angles (solar zenith angle, viewing zenith angle, and the relative difference azimuth). The original 31 land cover types were grouped into 14 categories (Table I) to represent major structural and surface cover combinations. For each land cover type, the clear-sky pixels were sampled using a regular grid, its size depending on the total number of clear-sky pixels for that land cover type. The total number of pixels per growing season was 40 000 (2000 per composite). For multiyear analysis (AVHRR, 1993 to 1996), 25% of the pixels in each of the above samples were selected and combined into one set. Different procedures were developed to derive model coefficients for each time period, land cover type, and spectral band. In the case of linear models (MWM, RM, RLM), a matrix inversion-based procedure solved the set of linear equations by minimizing an error function that measures the difference between estimated and observed values. It was implemented using LUT decomposition [34]. For NTAM, the nonlinear least square fit was computed using the modified Powell's minimization method [34]. Powell's iterative algorithm solves a multidimensional minimization problem as a sequence of operations that minimize function F along some vector direction n using Brent's bracketing method (see also [29]). The four BRDF models were compared for their ability to predict surface reflectance for a given viewing geometry. We used the coefficient of determination (r^2) and the standard error (se) to quantify the residual difference between predicted and observed surface reflectances. Predicted surface reflectances were computed using model parameters derived for three sampling periods: individual growing season, multiyear, and a ten-day period.

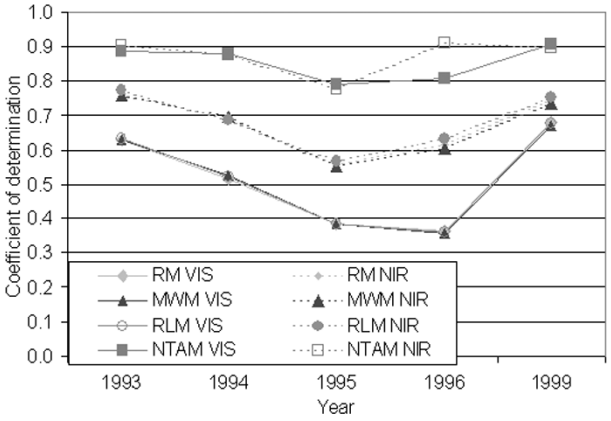

Fig. 3. Average (for 14 cover types) coefficients of determination r^2 between observed (independent variable) and estimated surface reflectance in AVHRR composite data.

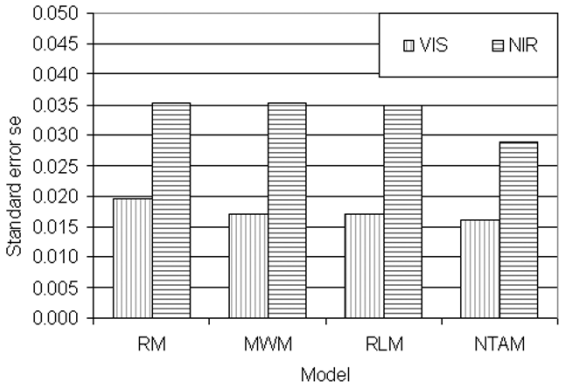

Fig. 4. Average (for 14 cover types) standard error se of AVHRR surface reflectance estimated by RM, MWM, RLM, and NTAM.

III. RESULTS AND DISCUSSION

A. Individual Growing Seasons

Fig. 3 shows average r^2 values obtained using data from five growing seasons with the four models and two spectral bands; each r^2 is an average for all 14 land cover types. The three linear models were very consistent but did not match the data as well as the nonlinear model. This is true for both AVHRR bands, although the linear models performed considerably better with NIR reflectance than with red. Fig. 4 shows the average standard error of the estimated surface reflectance se (1993 to 1996, 1999; all cover types) by spectral band.

Again, the standard error values were similar among the linear models, but higher than for NTAM. The same trends persisted in all years (not shown), although the absolute values differed. These results are not too surprising, since each sample

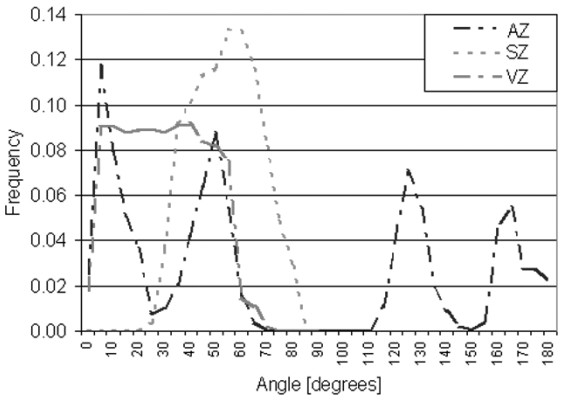

Fig. 5. Distribution of solar zenith, view zenith, and relative azimuth angles in the multiyear (1993 to 1996) sample of AVHRR composite data.

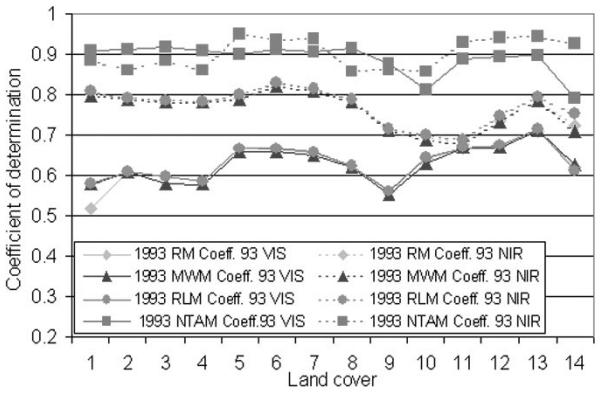

Fig. 6. Coefficients of determination r^2 for the plots of observed (independent variable) and estimated surface reflectance; the sample represents multiyear AVHRR composites of Canada for the 1993 to 1996 growing seasons.

encompassed data from the entire growing season, and the linear models were not able to cope with the changing target characteristics. Fig. 3 also shows that the interannual variations in r^2 were less pronounced for NTAM than for the three linear models. For MW, RLM, and RM, the amplitude of variations was greater in the red band than in NIR.

The reasons for the above trends are not fully clear, but in general, two principal causes may be considered: 1) deficiencies in the model formulation relative to the actual BRDF behavior and 2) noise in the observed reflectance. Regarding the second, the possible sources of the residual error could be variable accuracy of the georeferencing procedures, inaccuracies of input parameters applied in atmospheric corrections, and inaccurate cloud screening procedures. However, the relatively high and stable r^2 obtained for all seasons by NTAM (Fig. 4) suggests that differences in model formulation play a significant role. This does not support the often-encountered perception that semiempirical BRDF models for angular normalization are all similarly effective and that the research on this topic is mature.

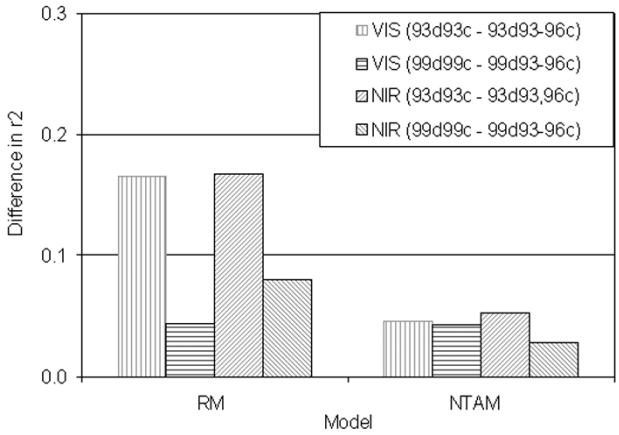

Fig. 7. Differences in r^2 between observed and estimated AVHRR surface reflectance caused by a temporal mismatch between data to be normalized and the model coefficients used in the normalization. Each linear regression represented by an r^2 is indicated by a symbol Y1dY2c, where Y1 is the period to which the coefficients were applied (e.g., 93d), and Y2 is the period from which they were derived (e.g., 93c).

B. Multiyear Data and Temporal Consistency

The four BRDF models were also evaluated by deriving model parameters from multiyear (1993 to 1996) data. The 1993 to 1996 period was selected because it encompasses a wide range of imaging geometries (including near-hotspot in 1994), and it also comprises two AVHRR sensors (onboard NOAA-11 and -14). In the combined dataset, the solar zenith angle values varied between 20° and 80° (Fig. 5), while the viewing zenith and relative azimuth angles spanned the full range of values. The behavior of the models in comparison to the observations is illustrated in Fig. 6 as r^2 between predicted and observed reflectances by land cover type. All models showed higher r^2 for the NIR compared to the visible band. Moreover, in the NIR, all four models yielded somewhat higher r^2 for forest cover types compared to open land. As for single years, NTAM yielded significantly higher r^2 values in both bands, for all cover types.

In addition to deriving model coefficients from a longer time series, we also considered the temporal stability of the model coefficients. This is a desirable characteristic because it facilitates near-real-time BRDF corrections after obtaining model coefficients from an existing dataset.

The model parameters were derived using a multiyear sample (1993 to 1996) and tested against model parameters derived for specific years, 1993 and 1999 ("target year"). The coefficients of determination (r^2) and standard errors (se) were computed for each land cover type between surface reflectance observed in the target year and reflectance estimated using parameters derived from: 1) the 1993 to 1996 sample or 2) the target year sample. Linear regressions were computed for 1993 data using 1993 model coefficients ($r^2_{93d,93c}$) and similarly using the 1993 to 1996 coefficients ($r^2_{93d,93-96c}$). Figs. 7 and 8 illustrate the behavior of RM (typical for the linear models) and NTAM in the above tests. Lower predictive power (corresponding to reduced r^2) is expected when model parameters derived from previous growing seasons are applied to subsequent periods. The decrease in r^2 values varied with year (Fig. 6): for NTAM, these were between 3% and 5% while for RM, they varied between 4% and 16%. The NTAM standard error increased by 0.01 [visible (VIS)] and 0.02 (NIR), while for RM, it increased by 0.04 (VIS) and 0.08 (NIR).

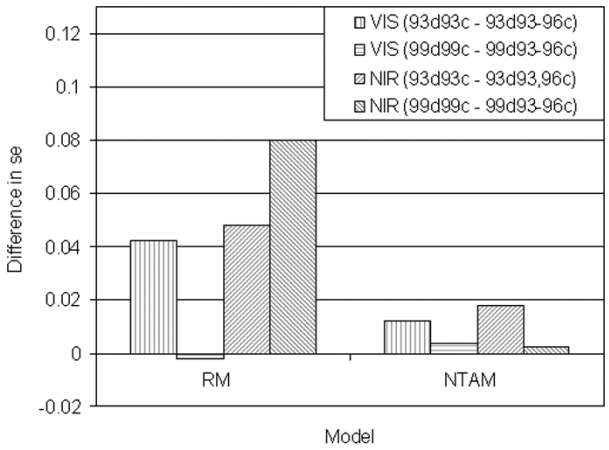

Fig. 8. Differences in the standard error of the estimated AVHRR surface reflectance caused by a temporal mismatch between data to be normalized and the model coefficients used in the normalization. Each linear regression is indicated by a symbol Y1dY2c, where Y1 the period to which the coefficients were applied (e.g., 93d), and Y2 is the period from which they were derived (e.g., 93c).

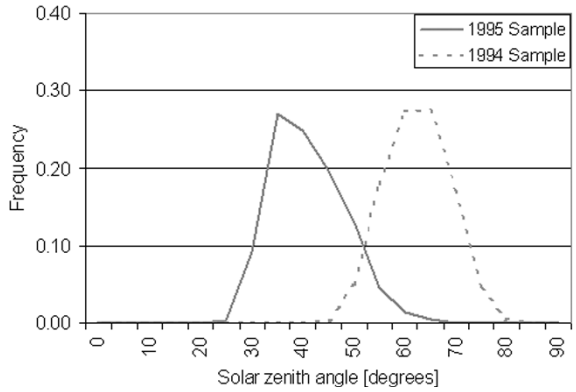

Fig. 9. Frequency distributions of solar zenith angle values in 1994 and 1995 AVHRR composite data.

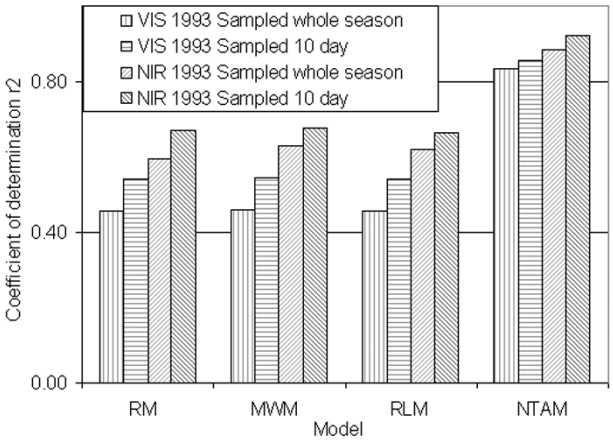

Fig. 10. Average coefficients of determination r^2 between observed and estimated AVHRR surface reflectance for 1993/08/1–10. Model parameters were derived for two sampling periods in 1993: ten days (1993/08/1–10) and the entire 1993 growing season.

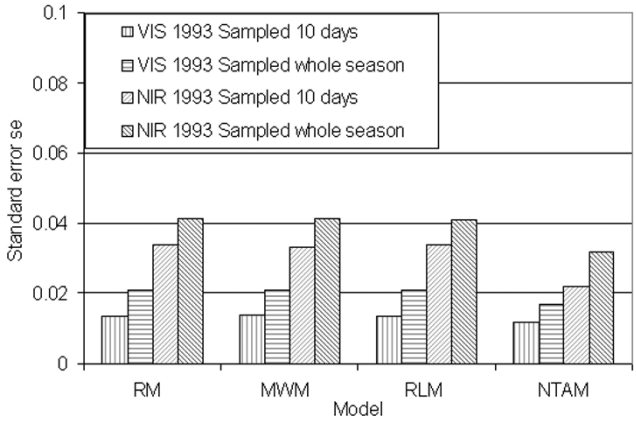

Fig. 11. Average standard error se for estimated AVHRR surface reflectance (period 1993/08/1–10). Model parameters were derived for two sampling periods in 1993: ten days (1993/08/1–10) and the entire 1993 growing season.

C. Model Behavior With Incomplete Sample

Two aspects were considered in this evaluation: an inadequate sampling of the measurement space and too few samples. The model's ability to extrapolate in the measurement space beyond the range of sampled values was tested using data from 1994 (NOAA-11, obtained around 1700 LST) and 1995 (NOAA-14, $\sim$ 1400 LST). The 1994 sample had a narrower range of sun zenith angles ($\sim 50^\circ$ to 80°, Fig. 9) than in 1995 ($\sim 30^\circ$ to 60°). Because of the difference in the θ_s range between these two years, the models are required to extrapolate well beyond the values with which the coefficients were estimated when 1995 data are simulated using model coefficients derived from 1994 dataset. Two sets of coefficients were derived for each model using samples from the 1994 and 1995 datasets, respectively. Surface reflectance observations in 1995 were estimated using these two sets of coefficients. To quantify the differences, r^2 and se were computed between surface reflectances observed in 1995 and the reflectances estimated by each set of coefficients (1994 or 1995).

NTAM was found to replicate both NIR and visible reflectance observations fairly well, with an overall r^2 of 0.79 for visible reflectance values based on 1994 coefficients ($r^2_{1995d,95c} = 0.84$). For NIR, NTAM r^2 was 0.77 with 1994 coefficients ($r^2_{1995d,95c} = 0.82$). The linear models were similar in magnitude but considerably lower, with a mean r^2 of 0.40 in NIR with 1994 coefficients ($r^2_{1995d,95c} = 0.55$). The standard error for NTAM for 1994 increased by 10% in the visible and 19% in the NIR, while the average increase for the linear models was 33% in the visible and 51% in the NIR band.

The majority of linear empirical models are not designed to cope with changing target characteristics. For most vegetation, reflectivity changes significantly during the growing season. Such models are then applied over short measurement periods so that the target remains approximately invariant while a sufficient number of samples are being collected. We compared the effectiveness of the four models using a ten-day (August 1–10, 1993) sampling period. To quantify the differences in performance, r^2 and se were computed between surface reflectances observed in 1993 (August 1–10) and reflectances estimated by each model using coefficients derived from 1) the ten-day sample and 2) the multiyear full-season sample (1993 to 1996). For both r^2 (Fig. 10) and *se* (Fig. 11), the results improved when the coefficients were derived for the short time period. The improvements were better for the linear models,

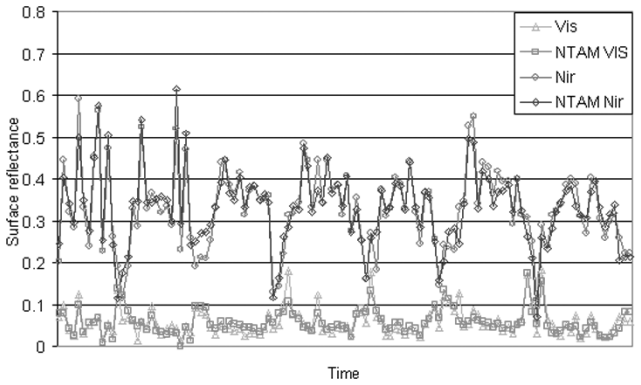

Fig. 12. Agreement between model predictions and observations in NIR and VIS band time series. A pixel, labeled as broadleaf mixed land cover type, is represented by AVHRR 1993 to 1999 time series.

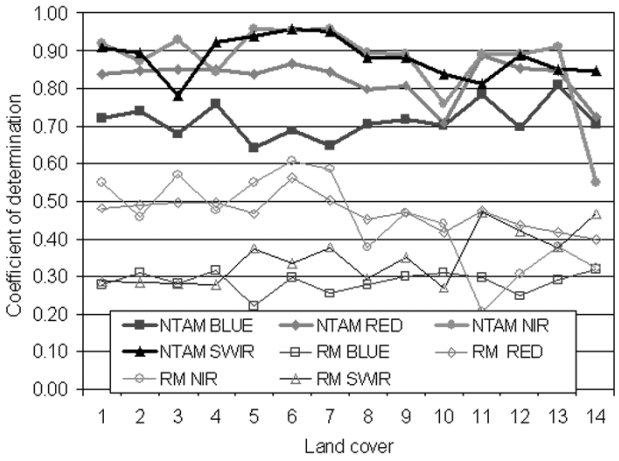

Fig. 13. Coefficients of determination r^2 for the plots of observed (independent variable) and estimated surface reflectance. The sample represents SPOT4/VGT composites of Canada for the 1999 growing season.

but not substantially so. As before, the highest r^2 was found for NTAM. On the other hand, all four models yielded comparable standard errors (Fig. 11).

Fig. 12 illustrates use of NTAM on a pixel basis. The figure shows an AVHRR surface reflectance time series of a randomly selected broadleaf mixed forest pixel in the VIS and NIR bands through the 1993 to 1999 growing seasons. Observations reveal a wide range of NDVI temporal variation due to phenological changes during the growing season as well the presence of variable sun-target-sensor geometry. One-half of the 140 available observations were used to derive the model coefficients. Fig. 12 shows good agreement between model predictions and observations in the NIR ($r^2 = 0.88$) and VIS ($r^2 = 0.71$) bands, which ensures normalization of the seven-year time series to a nominal viewing geometry: a crucial requirement for any multitemporal study.

D. Application of NTAM to VGT Data

The above comparison tests have shown that NTAM was able to account for the BRDF dependence of AVHRR surface reflectance more accurately than linear models. To test its suitability for other spectral bands and sensors, we have also used the procedure described in Section II-C for SPOT4 VGT data of Canada (1998 and 1999 seasons) and east Asia (1999).

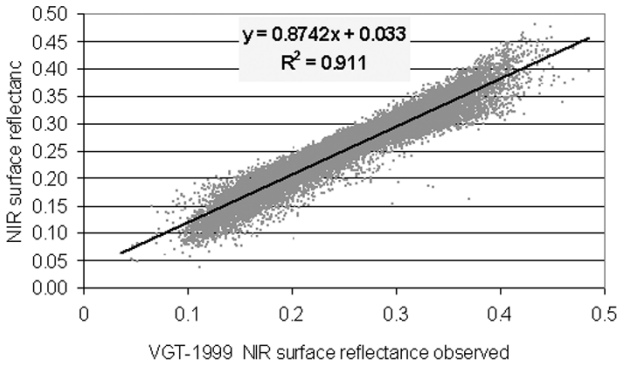

Fig. 14. Scatter plot of observed (SPOT4/VGT) and estimated (NTAM) NIR reflectance for broadleaf land cover over the 1999 growing season.

We derived the coefficients for RM and NTAM and compared the r^2 values for the 14 land cover types (Fig. 13). In general, r^2 values for both models were similar to those obtained for AVHRR data. The NTAM r^2 was consistently lower (by ~ 0.15) in the blue spectral band, possibly due to an increased effect of atmospheric scattering and attenuation. However, its performance in the SWIR band was as good as for the NIR band.

Fig. 14 shows close correspondence between observed and estimated NIR reflectance values of pixels across Canada for the whole 1999 growing season (broadleaf cover type).

IV. Discussion and Conclusion

The exploration of BRDF characteristics of land cover has three main applications: normalization of multiangle observations to a common viewing geometry, derivation of albedo from an angular integration of the BRDF, and derivation of biophysical and land cover properties from BRDF characteristics [20]. In this study, we compared the performance of recent linear BRDF models and a new nonlinear BRDF model (NTAM) for the normalization of multiangle observations. Based on several tests involving growing season AVHRR composite images over Canada between 1993 and 1999, we found relatively small differences among the linear models, but substantially better results for the nonlinear model. In all the tests undertaken, the nonlinear model yielded substantially better and more consistent results. NTAM also performed well for different sensors (AVHRR, VGT), geographic areas (Canada, east Asia), and spectral bands (blue to shortwave infrared). NTAM, thus, appears well suited for seasonally variable land cover types and a wide range of viewing geometries. The main reasons for NTAM's good performance ar 1) NTAM has sufficient number of coefficients to capture seasonal and interannual changes in targets and 2) the effects on BRDF of changes in the viewing geometry are well represented through the incorporation of a simplified hotspot function. The larger number of coefficients in NTAM compared to linear models is necessary if we are to normalize a time series of images with variable target characteristics.

In normalizing surface reflectance to a common geometry, there is a need for a consistent model with a defined set of coefficients that may be systematically applied to any dataset over a given geographic domain. We have demonstrated that this need can be met with NTAM or a similar nonlinear model that ac-

counts for temporal and spatial (within cover type) variability of the satellite signal. The "vegetation index surrogate" appears to be very effective in representing these factors.

In deriving NTAM model coefficients, we have employed a land cover map. However, knowledge of land cover is not necessary, as the basic requirement is for stratification of the pixels into a limited number of categories with distinct BRDF behavior. This could also be accomplished in other ways, such as through spectral clustering based on a vegetation index [19].

The temporal formulation of NTAM allows a time-invariant, single set of coefficients to be used in normalizing BRDF images acquired at any time during the growing season. Results of this study, thus, provide one approach to normalizing coarse- or medium-resolution data from instruments such as the NOAA AVHRR, SPOT/VEGETATION, MODIS, and the Medium Resolution Imaging Spectometer. For northern cover types, NTAM coefficients have been derived for AVHRR and VGT using the procedures described above, and they may be accessed at *ftp://ccrs.nrcan.gc.ca*. Since the model coefficients may be derived for any particular dataset, the procedures described here are readily applicable to other regions of the globe.

REFERENCES

[1] M. Barnsley, K. Morris, A. Strahler, and J. P. Muller, "Sampling the surface bidirectional reflectance distribution function (BRDF): Evaluation of current and future satellite sensors," *Remote Sens. Rev.*, vol. 8, pp. 893–916, 1994.

[2] J. M. Chen and J. Cihlar, "A hotspot in a simple bidirectional reflectance model for satellite applications," *J. Geophys. Res.*, vol. 102, pp. 25 907–25 913, 1997.

[3] J. Chen and S. Leblanc, "A four-scale bidirectional reflectance model based on canopy architecture," *IEEE Trans. Geosci. Remote Sensing*, vol. 35, pp. 1316–1337, Sept. 1997.

[4] J. Chen, G. Pavlic, L. Brown, J. Cihlar, S. G. Leblanc, P. White, R. J. Hall, D. Peddle, D. J. King, J. A. Trofymow, E. Swift, J. van der Sanden, and P. Pellikka, "Derivation and validation of Canada-wide coarse-resolution leaf area index maps using high-resolution satellite imagery and ground measurements," *Remote Sens. Environ.*, vol. 80, pp. 165–184, 2002.

[5] J. M. Chopping, "Large-scale BRDF retrieval over New Mexico with multiangular NOAA AVHRR dataset," *Remote Sens. Environ.*, vol. 74, pp. 163–191, 2000.

[6] J. Cihlar, I. Tcherednichenko, R. Latifovic, Z. Li, and J. Chen, "Impact of variable atmospheric water vapor content on AVHRR data corrections over land," *IEEE Trans. Geosci. Remote Sensing*, vol. 39, pp. 173–180, Jan. 2001.

[7] J. Cihlar, J. R. Latifovic, J. Chen, A. Trishchenko, Y. Du, G. Fedosejevs, and B. Guindon, "Systematic corrections of AVHRR image composites for temporal studies," *Remote Sens. Environ.*, 2003, to be published.

[8] J. Cihlar, R. Latifovic, J. Chen, and Z. Li, "Testing near-real time detection of contaminated pixels in AVHRR composites," *Can. J. Remote Sens.*, vol. 25, pp. 160–170, 1999.

[9] J. Cihlar, H. Ly, Z. Li, J. Chen, H. Pokrant, and F. Huang, "Multitemporal, multichannel AVHRR data sets for land biosphere studies: Artifacts and corrections," *Remote Sens. Environ.*, vol. 60, pp. 35–57, 1997.

[10] R. P. Entermont, C. B. Schaaf, W. Lucht, and A. H. Strahler, "Retrieval of red spectral albedo and bidirectional reflectance using AVHRR HRPT and GOES satellite observations of the New England region," *J. Geophys. Res.*, vol. 104, pp. 6229–6239, 1999.

[11] G. Fedosejevs, N. T. O'Neil, A. Royer, P. M. Teillet, A. I. Bokoye, and B. McArthur, "Aerosol optical depth for atmospheric correction of AVHRR composite data," *Can. J. Remote Sens.*, vol. 26, pp. 273–284, 2000.

[12] G. G. Gutman, "Global data on land surface parameters from NOAA AVHRR for use in numerical climate models," *J. Climate*, vol. 7, pp. 699–703, 1994.

[13] B. Hu, W. Lucht, A. H. Strahler, C. B. Schaaf, and M. Smith, "Surface albedos and angle-corrected NDVI from AVHRR observations of South America," *Remote Sens. Environ.*, vol. 71, pp. 119–132, 2000.

[14] M. Leroy and J. L. Roujean, "Sun and view angle correction on reflectance derived from NOAA/AVHRR," *IEEE Trans. Geosci. Remote Sensing*, vol. 32, pp. 684–697, May 1994.

[15] S. G. Leblanc, P. Bicheron, J. M. Chen, M. Leroy, and J. Cihlar, "Investigation of bidirectional reflectance of boreal forests using airborne POLDER and the 4-scale model," *IEEE Trans. Geosci. Remote Sensing*, vol. 37, pp. 1396–1414, May 1999.

[16] Z. Li, J. Cihlar, X. Zheng, L. Moreau, and H. Ly, "Bidirectional effects of AVHRR measurements over boreal regions," *IEEE Trans. Geosci. Remote Sensing*, vol. 34, pp. 1308–1322, Nov. 1996.

[17] X. Li and A. H. Strahler, "Geometric-optical bidirectional reflectance modeling of the discrete crown vegetation canopy: Effect of crown shape and mutual shadowing," *IEEE Trans. Geosci. Remote Sensing*, vol. 30, pp. 276–292, Mar. 1992.

[18] S. Liang, A. H. Strahler, M. J. Barnsley, C. C. Borel, S. W. Gerstl, D. J. Diner, A. J. Prata, and C. Walthall, "Multiangular remote sensing past, present and future," *Remote Sens. Rev.*, vol. 18, pp. 83–102, 2000.

[19] T. R. Loveland, B. C. Reed, J. F. Brown, D. O. Ohlen, Z. Zhu, L. Yang, and J. W. Merchant, "Development of a global land cover characteristics database and IGBP DISCover from 1 km AVHRR data," *Int. J. Remote Sens.*, vol. 21, pp. 1303–1330, 2000.

[20] W. Lucht and J. L. Roujean, "Considerations in the parametric modeling of BRDF and albedo from multi angular satellite sensor observations," *Remote Sens. Rev.*, vol. 18, pp. 343–379, 2000.

[21] W. Ni and X. Li, "A coupled vegetation-soil bidirectional reflectance model for a semiarid landscape," *Remote Sens. Environ.*, vol. 74, pp. 113–124, 2000.

[22] J. Qi, Y. H. Kerr, M. S. Moran, M. Weltz, A. R. Huete, S. Sorooshian, and R. Bryant, "Leaf area index estimates using remotely sensed data and BRDF models in a semiarid region," *Remote Sens. Environ.*, vol. 73, pp. 18–30, 2000.

[23] H. Rahman and G. Dedieu, "SMAC: A simplified method for atmospheric correction of satellite measurements in the solar spectrum," *Int. J. Remote Sens.*, vol. 15, pp. 123–143, 1994.

[24] J. L. Roujean, M. J. Leroy, and P. Y. Deschamps, "A bidirectional reflectance model of the earth's surface for the correction of remote sensing data," *J. Geophys. Res.*, vol. 97, pp. 20 455–20 468, 1992.

[25] W. Wanner, X. Li, and A. H. Strahler, "On the derivation of kernels for kernel-driven models of bidirectional reflectance," *J. Geophys. Res.*, vol. 100, pp. 21 077–21 089, 1995.

[26] W. Wanner, A. Strahler, B. Hu, P. Lewis, J.-P. Muller, X. Li, C. L. B. Schaaf, and M. Barnsley, "Global retrieval of bidirectional reflectance and albedo over land from EOS MODIS and MISR data: Theory and algorithm," *J. Geophys. Res.*, vol. 102, pp. 17 143–17 162, 1997.

[27] C. L. Walthall, J. M. Norman, J. M. Welles, G. Campbell, and B. L. Blad, "Simple equation to approximate the bidirectional reflectance from vegetation canopies and bare soil surface," *Appl. Opt.*, vol. 24, pp. 383–387, 1985.

[28] A. Wu, Z. Li, and J. Cihlar, "Effects of land cover type and greenness on advanced very high resolution radiometer bidirectional reflectance: Analysis and removal," *J. Geophys. Res.*, vol. 100, pp. 9179–9191, 1995.

[29] Z. Zhang, S. N. V. Kalluri, J. J. S. Liang, and J. R. G. Townshend, "Models and high – performance algorithms for global BRDF retrieval," *IEEE Comput. Sci. Eng.*, vol. 5, pp. 16–29, 1998.

[30] P. J. Sellers, B. W. Meeson, F. G. Hall, G. Asrar , R. E. Murphy , R. A. Schiffer, F. P. Bretherton, R. E. Dickinson , R. G. Ellingson , and C. B. Fidol, "Remote sensing of the land surface for studies of global change: Models—Algorithms experiments," *Remote Sens. Environ.*, vol. 51, no. 1, pp. 3–26, Jan. 1995.

[31] J. Cihlar and P. M. Teillet, "Forward piecewise linear calibration model for quasireal time processing of AVHRR data," *Can. J. Remote Sens.*, vol. 21, pp. 22–27, 1995.

[32] B. Robertson, A. Erickson, J. Friedel, B. Guindon, T. Fisher, R. Brown, P. Teillet, M. D'Iorio, J. Cihlar, and A. Sancz, "GeoComp, a NOAA AVHRR geocoding and compositing system," in *Proc. ISPRS Conf., Commission 2*, Washington, D.C, 1992, pp. 223–228.

[33] J. Cihlar, J. Beaubien, R. Latifovic, and G. Simard, "Land cover of Canada 1995," Natural Resources Canada, Ottawa, ON, Ver. 1.1. Digital Data Set Doc., 1999.

[34] H. W. Press, A. T. Teukolsky, T. W. Vetterlin, and P. B. Flannery, *Numerical Recipies in C: The Art of Scientific Computing*. Cambridge, U.K.: Cambrige Univ. Press, 1992.

[35] "Meteor-3 Total Ozone Mapping Spectrometer (TOMS) data products user's guide," NASA Goddard Space Flight Center, Greenbelt, MD, 1996.

[36] E. Kalnay, M. Kanamitsu, R. Kisler, W. Collins, D. Deaven, L. Gandin, M. Iredell, S. Sasha, G. White, J. Woolen, Y. Zhu, M. Chelliah, W. Ebisuzaki, W. Higgins, J. Janowiak, K. C. Mo, C. Ropelewski, J. Wang, A. Leetmaa, R. Reynolds, R. Jenne, and D. Joseph, "The NCEP/NCAR 40-year reanalysis project," *Bull. Amer. Meteorol. Soc.*, vol. 77, pp. 437–471, 1996.

Rasim Latifovic received the B.S. degree in mining engineering from the University of Tuzla, Tuzla, Yugoslavia, in 1982, and the M.S. degree in technical science from the University of Belgrade, Belgrade, Yugoslavia, in 1989. He is currently pursuing the Ph.D. degree at the University of Laval, Quebec City, QC, Canada.

He is currently a Physical Scientist with Canada Center for Remote Sensing, Natural Resources Canada, Ottawa, ON. His current research includes the application of multitemporal and multiresolution satellite data, including all other aspects of remote sensing for environmental impact assessment and monitoring. Until 1995, he taught at the University of Tuzla, and carried research in the areas of mathematical modeling in geology and mining, descriptive geometry, mapping, and computer graphics.

Josef Cihlar received graduate degrees in soil and geography science.

He is currently a Senior Research Scientist and Program Manager of the Climate Change Programme of the Earth Science Sector, Natural Resources Canada, Ottawa, ON. His primary research interests are in the use of satellite observations to understand the dynamics of terrestrial ecosystems, especially their roles in the global carbon and hydrological cycles. He leads a team of research scientists engaged in developing techniques and models for the quantitative use of earth observation data in understanding, monitoring, and assessment of the terrestrial environment, with emphasis on boreal ecosystems. He is involved in numerous international programs dealing with global observation, including the Global Terrestrial Observing System and the Global Climate Observing System. Since 1999, he has co-led the development of terrestrial carbon observation scheme for the Integrated Global Observing Strategy Partnership (IGOS-P).

Dr. Cihlar has received numerous awards, including the Head of Public Service Award in 1998. He was elected Fellow of the Royal Society of Canada in 2000, and Fellow of the Canadian Aeronautics and Space Institute in 2002. In December 2002, he was appointed Program Manager for the Climate Change Program of the Earth Sciences Sector, Natural Resources Canada.

Jing Chen (M'01) received the B.S. degree from the Nanjing Institute of Meteorology, Nanjing, China, in 1982, and the Ph.D. degree in meteorology from Reading University, Reading, U.K., in 1986.

He is currently a Professor in the Department of Geography at the University of Toronto, Toronto, ON, Canada, as well as an Adjunct Professor at York University, York, U.K. From 1989 to 1993, he was a Postdoctoral Fellow and Research Associate with the University of British Colombia, BC, Canada. From 1993 to 2000, he was a Research Scientist with the Canada Centre for Remote Sensing, Ottawa, ON. His research interests are in remote sensing of the biogeophysical parameters, plant canopy radiation models, and terrestrial water and carbon cycles. He is the author of over 90 papers in refereed journals, with approximately 150 scientific/technical publications.

Dr. Chen was Associate Editor of the IEEE TRANSACTIONS ON GEOSCIENCE AND REMOTE SENSING from 1996 to 2002.